Article citation info:
Witaszek K, Witaszek M. Diagnosing the thermostat using vehicle on-board diagnostic (OBD) data. Diagnostyka. 2023;24(4):2023402. https://doi.org/10.29354/diag/173002.

DIAGNOSTYKA, 2023, Vol. 24, No. 4

e-ISSN 2449-5220
DOI: 10.29354/diag/173002

DIAGNOSING THE THERMOSTAT USING VEHICLE ON-BOARD DIAGNOSTIC (OBD) DATA

Kazimierz WITASZEK [1, *], Mirosław WITASZEK [1]

[1] Silesian University of Technology, Faculty of Transport and Aviation Engineering, Krasińskiego 8, 40-019 Katowice, Poland
[*] Corresponding author: e-mail: kazimierz.witaszek@polsl.pl

Abstract

The thermostat is a crucial component of a car's internal combustion engine's cooling system. Failure of the thermostat can result in undercooling or overheating of the engine. Undercooling may increase wear of engine components due to poor lubrication and lead to higher fuel consumption. Conversely, overheating can damage the engine. The engine coolant temperature is one of the fundamental parameters for the proper functioning of the engine. The vehicle's onboard diagnostics system was unable to detect the malfunction of the thermostat. As a consequence, fuel consumption increased, which was especially noticeable in winter. This paper evaluates the possibility of carrying out thermostat diagnostics using data obtained from the OBD system through a diagnostic interface ELM327, which is connected to the OBD-II connector and interfaced with Torque Pro software on a smartphone. Analysis of the data confirmed that the proposed diagnostic method was appropriate. Furthermore, the impact of the thermostat malfunction on different factors such as coolant temperature, cold engine warm-up time, parameters characterising thermostat cycling, and fuel consumption of the car were studied. It was found that, apart from the already mentioned decrease in coolant temperature, the thermostat hysteresis also decreased and the thermostat cycle time increased.

Keywords: thermostat, diagnostics, malfunction, coolant temperature, fuel consumption

List of Symbols/Acronyms

$*_I$ – value or function for previous car;
$*_{II}$ – value or function for car with faulty thermostat;
$*_{II}$ – value or function for car with replaced thermostat;
A – engine start point;
AB – cold engine warm-up phase;
a_i – function parameter;
B_1 – end of engine warm-up point (first thermostat opening);
B_i – thermostat opening points;
b_i – function parameter;
BC – hot engine cooling phase (open thermostat cycle);
C_i – thermostat closing points;
c_i – function parameter;
CB – hot engine heating phase (closed thermostat cycle);
ΔT_{BC} – thermostat operating hysteresis [°C];
Δt_{CC} – thermostat cycle time [s];
ECU – Engine Control Unit;
ELM327 – diagnostic interface for OBD-II;
$f_{AB\_i}(t)$ – function for the engine warm-up phase;
$f_{BC\_i}(t)$ – function for the engine cooling phase;
$f_{CB\_i}(t)$ – function for the engine heating phase;
$f(t)$ – thermostat model function;
FPC – Free Pascal Compiler;
GPS – Global Positioning System;
n – data volume
OBD-II – on-board diagnostic level 2 interface;
R^2 – square of the correlation coefficient;
RTC – Real Time Clock;
RMSE – Root Mean Square Error
SSE – Sum of Squared Errors;
SSE_C – Sum of Squared Errors for cycle;
SSE_T – Sum of Squared Errors for certain temperature;
σ_T – temperature standard deviation [°C];
T – engine temperature [°C];
t – time [s]
T_A – initial engine temperature [°C];
T_{avg} – average engine temperature [°C];
T_{avgB1} – average first thermostat opening temp. [°C];
T_{avgBi} – average thermostat opening temperature [°C];
T_{avgCi} – average thermostat closing temperature [°C];
t_{avgT} – average time coordinate for a set of points at a given temperature T [s];
T_{B1} – first thermostat opening temperature [°C];
T_{Bi} – thermostat opening temperature [°C];
T_{Ci} – thermostat closing temperature [°C];
t_i – time coordinate of temperature measurement [s];
T_{min} – minimum engine temperature [°C];
T_{max} – maximum engine temperature [°C];
T_{Q1} – first quartile engine temperature [°C];
T_{Q2} – median engine temperature [°C];
T_{Q3} – third quartile engine temperature [°C];
v_i – rate of engine heating or cooling [°C/s];
$v_{i\ min}$ – minimum rate of engine heating or cooling [°C/s];
$v_{i\ max}$ – maximum rate of engine heating or cooling [°C/s];
$v_{i\ avg}$ – average rate of engine heating or cooling [°C/s].

Received 2023-08-23; Accepted 2023-09-28; Available online 2023-09-29

1. INTRODUCTION

Despite the efforts to promote the wide usage of electric cars, the majority of modern cars are still powered by internal combustion engines [11]. Internal combustion engines are also used in agricultural machinery, ships, airplanes, and rail transportation, making vehicle fuel consumption the largest contributor to energy consumption in the transportation sector [5, 18]. Therefore, efforts are being made to improve internal combustion engines [8, 12, 15, 17]. The efficiency of these engines does not exceed 22%-45% [8, 15, 23]. As for heavy-duty diesel engines, their efficiency can go beyond 50% [22]. A significant amount, around 22% to 35%, of the energy supplied to the engine with the fuel is lost in engine cooling, mainly through the cooling system [15, 23]. The cooling system directly influences engine service life, efficiency, fuel consumption, and emissions [3, 12, 24]. Work is underway to improve this system through the use of additional electrical and electronic systems: sensors, control units, electric servomotor actuators, smart thermostats or electric coolant pumps [1, 3, 16, 21, 24].

The thermostat plays an important role in the cooling system. Traditional wax thermostats react slowly to abrupt changes in engine heat load causing undesirable temperature fluctuations, which reduces engine efficiency [16]. The use of electrically controlled valves instead of traditional thermostats improves coolant flow control and reduces flow resistance [16]. This improves engine efficiency and reduces the power requirement for the engine's cooling system. As a result, the engine's fuel consumption decreases. According to the results presented in work [3], using a modern electronic thermostat instead of a conventional mechanical one resulted in reducing fuel consumption by 1.7%. The article [16] shows that the use of such thermostat significantly reduces the emission of harmful components (hydrocarbons, carbon monoxide, particulate matter) and greenhouse gases (CO_2) in the exhaust gases of light diesel vehicles. However, a slight increase in nitrogen oxide - NO_X emissions was observed. Using an electronic thermostat also reduced the test engine's warm-up time, resulting in reduced cold start emissions [1, 16].

The design of cooling systems is not the only area where improvements are being made. Research into new coolants for automotive combustion engines is also underway. These fluids have improved thermal properties and reduced environmental effects. For this purpose, fluids are used that contain nanoparticles with a size ranging from 1 nm to 100 nm [6, 7, 14]. Compared to traditional fluids such as water, ethylene glycol or oil, these fluids have significantly higher heat transfer and convective heat transfer coefficients [6, 7, 14]. Often their use does not result in a significant increase in pumping losses [7, 14]. Cooling liquids like these are used in a wide variety of applications such as electronic components, heating and cooling systems, photovoltaics, and nuclear reactors [7, 26]. In automobiles, these fluids help downsize radiators, improving vehicle aerodynamics and reducing aerodynamic coefficient of drag [6, 14]. Further reductions in fuel consumption and improvements in car fuel efficiency are achieved through this process [6, 14].

Fuel consumption, along with engine horsepower or torque, is a crucial parameter that characterises the efficiency of engine operation and the technical condition of the drivetrain [20]. It varies depending on the car's operating conditions. For instance, driving in urban traffic conditions - characterised by short travel distances, frequent acceleration, or underheating of the engine - increases fuel consumption [20].

The ambient temperature significantly impacts fuel consumption. According to a study on fuel consumption of passenger cars [4, 20], a drop in ambient temperature from 13ºC to -1ºC led to a 36.5% increase in fuel consumption, and a decrease in outdoor temperature from 5ºC to -15ºC resulted in a 34.9% increase in fuel consumption. Similarly, high ambient temperatures increase fuel consumption, for instance, due to the use of air conditioning. The paper [20] reports that the car observed showed a 42.3% increase in fuel consumption when the temperature rose from 13ºC to 26ºC.

Engine temperature is a critical operational parameter. Going above the optimal temperature level can damage the engine [6]. Overcooling a car engine can lead to increased fuel consumption due to increased inefficiency [9, 21]. This results in higher emissions of harmful air pollutants [9, 12, 16, 24]. Low engine temperatures cause the oil viscosity to increase and worsen the lubrication of engine components, resulting in increased mechanical losses and wear rate of engine parts [15, 19]. Coolant temperature and cold engine warming-up time can serve as parameters for characterizing the thermal conditions during engine operation [16]. The coolant temperature changes depending on the engine operating conditions, such as its load, rotational speed of crankshaft, and the ambient temperature. [13]. The thermostat is a crucial component in determining the coolant temperature [3, 16].

Modern cars use automatic control and diagnostic systems based on programmable microcontrollers [2, 3, 25]. The effectiveness of self-diagnostic systems in a given vehicle relies on meeting regulatory demands and anticipating potential failures during the design stage of the car [10]. These systems can effectively identify common faults, which are then reported to the driver via indicators and text messages.

A device that informs the driver of the current engine coolant temperature and warns if it exceeds the maximum value is installed to continuously monitor the engine's operating temperature. It is typically mounted on the car's dashboard. In the past, mechanical gauges with pivoting pointers were

commonly used (Fig. 1a). Currently, there is a preference among manufacturers to use digital dashboards with displays (Fig. 1b). However, this approach has led to a reduction in the amount and detail of information provided to the driver in certain car models. In some cases, no indication of the current engine operating temperature is given in cars, with only indicator lights warning that the temperature has been exceeded (Fig. 1c).

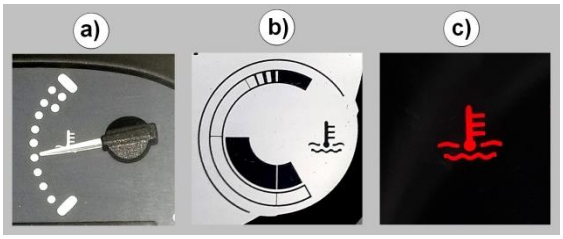

Fig. 1. Examples of types of automotive engine temperature indicators:
a) analog (Renaut Thalia I 2003)
b) digital (Renault Megane III 2014)
c) indicator light (Ford Fiesta VI 2011)

For some time, cars have been equipped with digital interfaces which allow additional diagnostic devices to be connected, leading to a significant improvement in the ability to diagnose faults [2, 25]. An example of such a connector is the OBD-II (On-Board Diagnostic level 2) socket.

The purpose of this paper is to investigate the diagnostic capabilities of the thermostat using data obtained from the engine control unit via a diagnostic interface connected to the OBD-II socket. Furthermore, the impact of thermostat malfunction on coolant temperature, cold engine warming-up time, and changes in temperature during the thermostat cyclic operation of the thermostat in a passenger vehicle, were studied.

2. CASE STUDY

This article is based on a case of thermostat failure in a Reanult Megane III Grandtour car manufactured in 2014. It is equipped with a K4M 1.6 VVT 110 spark-ignition internal combustion engine with displacement volume of 1598 cm^3 and maximum power of 82 kW. Car was purchased in September 2021 and is still in operation today. It replaced a car that was four years older and had the same engine as the new one.

2.1. Failure symptoms

The test vehicle operated without any symptoms that could be considered alarming to the driver. There was no loss of power, nor were there any unusual noises, smells or smoke from the exhaust system. The car's OBD system reported no faults or warnings. However, a slight increase in fuel consumption compared to the previous car was observed during continuous monitoring. During winter months and lower outside temperatures, there was a noticeable increase in average fuel consumption as reported by the on-board computer (Fig. 2).

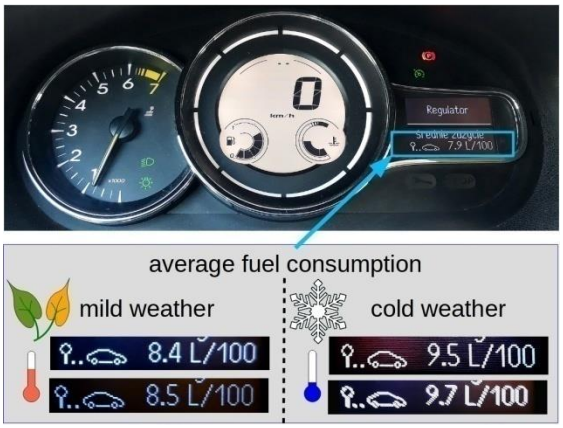

Fig. 2. On-board computer messages

The tachometer is the only analogue instrument on the Renault Megane III dashboard, with all other information displayed on LCD screens. One of these features is the engine operating temperature indicator, as shown in Figure 3. During typical vehicle operation, the indicator shows one of three possible states. Immediately after starting a cold engine, all segments of the indicator are blank (Fig. 3a). When the engine temperature reaches 50°C, the first, lowest segment is switched on (Fig. 3b). As the engine warms up, the status of the indicator remains constant. When the engine coolant temperature reaches 80°C, the system activates the next longest segment, resulting in two active segments (Fig. 3c).

Fig. 3. Operating states of the engine coolant temperature indicator of the Renault Megane III car

During long journeys the indicator usually showed that the engine had reached its optimum operating temperature. However, there was sometimes noticeable momentary fading in and out of the second segment of the indicator, which may suggest that the engine's operating temperature was too low.

2.2. Initial fault diagnosis and repair

The symptoms described in paragraph 2.1 prompted the vehicle owner to carry out a diagnostic tests to confirm the correct operation of the engine cooling system.

An OBD-II diagnostic socket was used to communicate with the engine control unit (ECU) and

read stored fault codes. This socket was connected to a BOSCH KTS 590 diagnostic tester, which read the fault memory, but no entry was found relating to engine operation and temperature. In addition, the ELM327 diagnostic interface and Torque Pro software were used to collect data on the vehicle and engine operation from the start of the vehicle's operation. The data monitored included engine coolant temperature. Observations of the coolant temperature showed it typically reached 80°C. This was slightly lower than the values typically observed in the previously used car. Based on these indications, a thermostat malfunction was suspected and the car workshop was instructed to check and make the necessary repairs.

The diagnosis at the workshop did not confirm any apparent malfunction although the possibility of a partially malfunctioning thermostat could not be excluded, given the described symptoms. In conclusion, the thermostat was replaced with a new one based on a reasonable suspicion that the old one was not functioning properly. On the K4M engine it is necessary to replace the entire assembly, including the housing and temperature sensor, as it is not possible to remove only the thermostat. The thermostat housing is bolted to the engine head and contains channels for both coolant and oil. Figure 4 shows a view of the thermostat assembly after it has been removed from the engine.

Fig. 4. K4M engine thermostat assembly

3. VERIFICATION OF THE REPAIR

The repair was carried out in June 2022. After the repair, engine performance data was continuously recorded via the OBD-II socket, and photographs were taken of the odometer, on-board computer messages and fuel distributor readings each time the vehicle was refuelled. Based on the data obtained in this way, it was decided to evaluate the results of the repair. This evaluation was based on a comparison of the car's operating data before and after the repair, as well as with data from the previously operated car.

3.1. Data acquisition from the OBD-II interface

Each car used by one of the authors was equipped with a system for recording data relating to the vehicle's functioning after purchase. The system used the standard car OBD-II socket. Before driving, the author connected an ELM327 diagnostic interface, a cheap but handy device, to this socket. The ELM327 is commonly used to obtain fault messages from the car's engine control unit (ECU), and helps with engine diagnostics. Clearing error memory is an option but should only be done after checking the fault code and fixing the underlying problem. This diagnostic interface is not a stand-alone device and requires the appropriate software on a PC, tablet or smartphone to operate. If specific software is chosen, an ELM327 interface-based test system can be enhanced to include cyclic reading and, more importantly, recording of current engine and vehicle operating parameters. Communication between the unit and the software is usually wireless via Bluetooth. Interfaces with WiFi or USB connections are also available. Specialised applications are available to run the ELM327 on different operating systems. The Samsung Galaxy S4 Mini Smartphone (GT9195) was chosen to operate the ELM327 due to its ease of use, compact size, portability and space-saving design. The device operates on the Android 4.4.2 operating system with kernel version 3.4.0-4770408. The GT9195 smartphone had already proven its effectiveness in the same application in a previously operated vehicle.

The Torque Pro application, available from the Google Play store, was chosen for its data logging features and particularly its auto-starting capability. Compared to the free version of Torque, this application offers significantly more configuration options for the data logging system. The system was configured to log engine parameters once per second.

The measured data was stored in the phone's internal memory. The information came from several sources. The vehicle's OBD-II system, which provided current engine and powertrain parameters, was the primary source. Another data source was the GPS satellite system. This provided the vehicle's position and speed. The GPS module was part of the smartphone itself. In addition, other data such as the current time from real time clock (RTC) and accelerations were obtained from the smartphone's internal modules.

The constant use of the GPS and Bluetooth modules increases battery consumption. This could lead to battery drain during long trips. In addition, the smartphone was powered by the Reinston EPB019 10000 mAh power bank via a micro-USB connector.

Figure 5 shows the scheme of the measurement system. The data collected while driving was continuously stored in the non-volatile memory of the smartphone. Periodically, the data was downloaded to a desktop computer via USB.

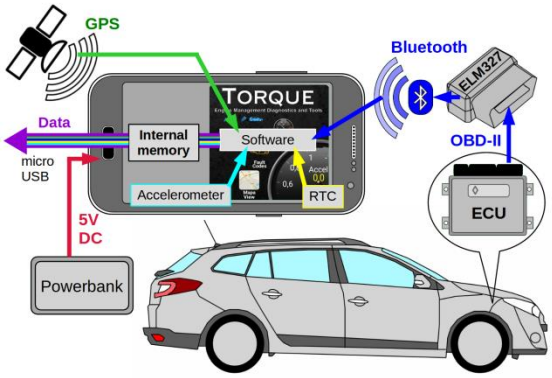

Fig. 5. Scheme of the data acquisition system

To protect the data from potential loss, additional copies were made on SD cards and stored on external media. Data were collected from the majority of routes travelled by vehicles.

3.2. Processing and analysis of OBD data

The measurement system is set up to open a new file for each run of Torque programme, with a file name that encodes the date and time information. The file naming convention is as follows:

trackLog-YYYY-MTH-DD_HH-MM-SS.csv,

where: YYYY stands for the year, MTH for the month, DD for the day, HH for the hours, MM for the minutes and SS for the seconds.

Measurement data is stored in text files with the csv extension (*.csv). This allows tools such as spreadsheets to be used to analyse the data files. While this approach is effective for analysing a small number of files, it would require significant manual effort to perform a more comprehensive analysis. To address this issue, some customised software tools were developed, namely OBD_T5c.exe, Coolant.exe, TimeShift.exe, and Histogram.exe, which could process a large number of data files without user interaction by operating in batch mode. As there was no requirement for a comprehensive user interface with this mode of operation, all programs were written in Pascal and compiled using the Free Pascal Compiler (FPC) ver. 3.0.4. Console scripts were also developed to provide a range of system commands for executing the above programs.

Data in trip log files is recorded sequentially in rows. Each line is an independent data record and contains information from the OBD system, GPS and smartphone sensors. During every journey, 28 parameters were recorded. The analysis of thermostat performance was based on a subset of these parameters, while the rest were collected for parallel research.

The first step in the data analysis was to select and aggregate data from the trip log files. This is shown schematically in Figure 6. The software program OBD_T5c.exe, developed specifically for this purpose, was used. This program, when launched, reads successive records from the trip logs (*.csv), processes the data lines and decodes the contents of the corresponding variables.

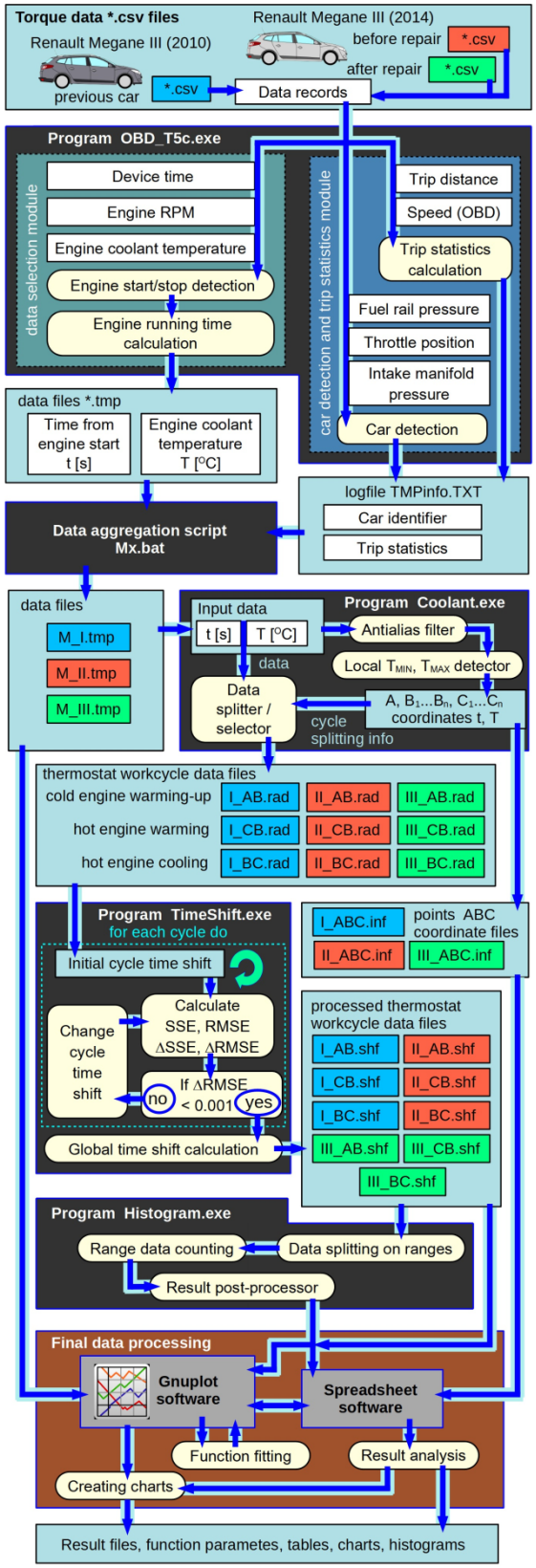

Fig. 6. Scheme for processing test data read from OBD-II system

Two types of processing were performed on the data from the input files. Most important was

extracting information related to engine coolant temperature changes over time. This information was stored in text format in the *.tmp files produced as output. The data lines consisted of two fields: time and the corresponding engine temperature. The temperature readings were filtered to be written only when the engine was running.

Engine operation was detected on the basis of a logical condition: engine speed value greater than 0. A new data series was written to the output file for each engine restart. A blank line was used to separate the series. The header lines were preceded by a # character. This organisation of the output files allowed easy merging and further analysis in the future.

In addition, the OBD_T5c.exe program read other data from the input files. The values of certain parameters, such as intake manifold pressure, fuel rail pressure and throttle position, were used to identify the vehicle from which the logbook originated. Other record fields were used to calculate general data characterising each research period, as shown in Figure 7.

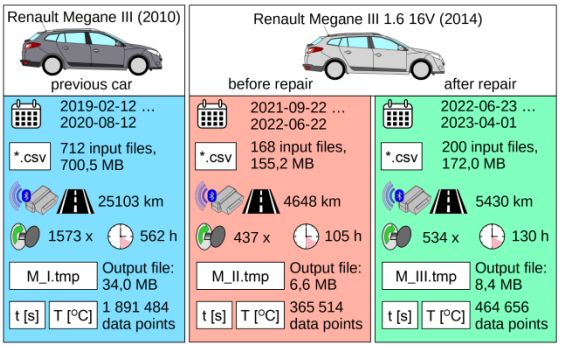

Fig. 7: Characteristics of the data recorded during the study

The OBD_T5c result files were merged into three files using the Mx.bat console script. Each file contained the filtered data from the corresponding period of the research. Using the data prepared in this way, histograms of the engine temperatures recorded during vehicle operation were generated, as shown in Figure 8.

Figure 8a shows the engine temperature histogram of the previously used vehicle and Figure 8b shows that of the currently used vehicle. The red colour represents the data for the pre-repair condition. While the green colour corresponds to the data collected after the repair. From Figure 8 it can be concluded that before the repair, the operating temperature of the engine with the faulty thermostat was most often in the range of 75-76°C. This is a slightly below the optimum values. After replacing the thermostat with a new one, the engine generally operated at 10°C higher temperature, between 85-86°C. The pre- and post-repair histograms are clearly separated, with only a small common area. From this it can be concluded that the replacement of the thermostat had a significant effect on the temperature conditions of the engine.

The previously operated 2010 Renault Megane most often showed an engine temperature of 83-84°C (Fig. 8a), that is, only slightly lower than the newer vehicle after thermostat replacement.

The basic statistics of the measurements recorded are presented in Table 1.

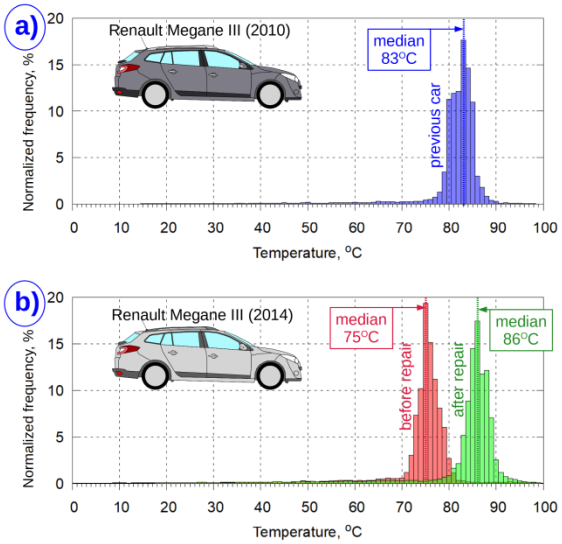

Fig. 8. Engine operating temperature histograms of the tested vehicles

Table 1. Basic measurement data statistics

Parameter		Renault Megane III (2010) previous car	Renault Megane III (2014) before repair	Renault Megane III (2014) after repair
Data volume n		1891484	365514	464656
Temperatures [°C]	Minimum T_{min}	0	-2	0
	Maximum T_{max}	99	99	99
	Average T_{avg}	80,34	72,98	82,62
	Standard deviation σ_T	9,52	10,86	11,78
	First quartile T_{Q1}	80	74	84
	Median T_{Q2}	83	75	86
	Third quartile T_{Q3}	84	77	88

Table 1 shows that the average temperature value T_{avg} calculated from engine start is usually below the first quartile. This is because the average calculation includes the cold engine warm-up data. It is better to deduce the engine operating temperature from the median temperature T_{Q2}. Furthermore, when the median temperature values are plotted on histograms (see Figure 8), it is seen that they coincide with the bar representing the most frequent data.

The temperature distribution functions derived from the histograms are shown in Figure 9. It can be seen that for the range of results between 15% and

90%, the curves for the newer car, before and after repair, are shifted by about 10°C. In the same range the distribution functions for the previously used car and the newer car after repair are shifted by about 3°C. These results confirm that there is a significant change in engine operating temperature after thermostat replacement.

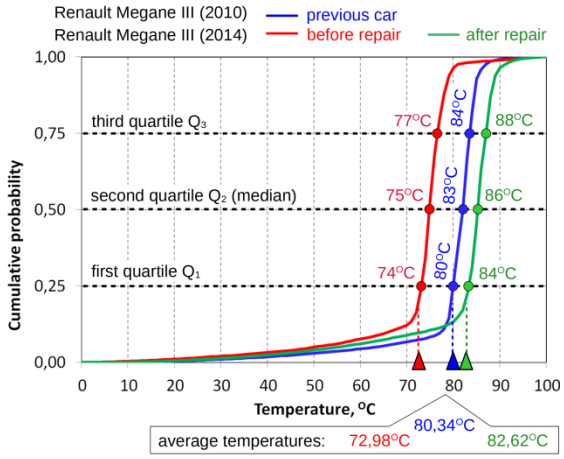

Fig. 9. Operating temperature distribution functions of the of the tested vehicles' engines

Next, the data sets were divided into subsets containing data from each characteristic phase of the engine temperature control system. Figure 10 shows engine temperature variation over 700 seconds. In the initial phase, after starting the engine (point A), the cold engine gradually heats up until the first thermostat opens (point B_1). Next, the diagram shows the cyclical changes in engine temperature associated with the thermostat opening and closing the flow of coolant through the engine radiator. These phases correspond to the temperature drop cycles that occur between the opening (B_i) and closing (C_i) points of the thermostat. These are followed by temperature rise cycles starting at points (C_i) and ending at points (B_{i+1}).

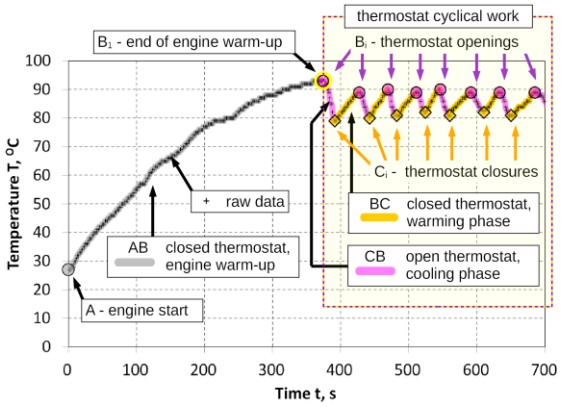

Fig. 10. Example of engine temperature variation during 700 s of operation with characteristic points marked

The data from each of the three research periods were further divided into three sub-sections:

- cold engine warm-up (AB),
- hot engine cooling phase (BC),
- hot engine heating phase (CB).

The data were separated using a custom-built program called Coolant.exe (Fig. 6). An anti-aliasing filter was used at this stage to average the data over time intervals. Coolant.exe generated data for all relevant points in the temperature curve, i.e. points A, B and C. This facilitated the identification of local minima and maxima in the temperature curve, i.e. points B and C.

Sufficient data collected from several comparable runs can be used to formulate mathematical functions that describe the characteristics of the temperature-time curve. The successive cycles of engine temperature changes recorded during the tests consist of many measurement points grouped by temperature. This phenomenon is called aliasing and is caused by the relatively low resolution of the engine temperature measurement by the ECU, which is 1 degree Celsius. The successive cycles of the thermostat are, of course, shifted in time, as can be seen in Figure 11a. It was therefore necessary to develop a program called TimeShift.exe which, by successive approximations, determined the optimum time shift for the entire cycle, ensuring the highest possible concentration of results for all recorded cycles without altering the nature of the curves. The algorithm worked by calculating the average time coordinate, t_{avgT}, for a set of points, t_i, at a given temperature T. The algorithm then determined the sum of squared errors (SSE_T) for this set of points using formula (1).

$$SSE_T = \sum_{i=1}^{n_T} \left(t_i - t_{avgT}\right)^2 \tag{1}$$

The calculations covered the temperature range common to both runs being compared. They were performed sequentially for all groups of results in both runs over the range T_{min} to T_{max}. The sum of squared errors for the compared thermostat cycles (SSE_C) was obtained by summing their results using formula (2).

$$SSE_C = \sum_{j=Tmin}^{Tmax} SSE_{Tj} \tag{2}$$

Equation (3) was used to calculate the final sum of squared errors (SSE) in all analysed thermostat cycles.

$$SSE = \sum_{C=1}^{Cn} SSE_C \tag{3}$$

Using equation (4) and the total number of measurement points (n), the root mean square error ($RMSE$) was then calculated.

$$RMSE = \sqrt{\frac{SSE}{n}} \tag{4}$$

The program's algorithm used a method of successive approximations to calculate the optimum time shifts for all compared runs. This minimised the $RMSE$ error. The current phase of the program's

operation ended when the *RMSE* error changed less than 0.001 in successive iterations of the calculation loop. Following the calculation of the optimal shifts for all cycles in a given dataset, a global time shift was applied to ensure that the first point on the left obtained a zero time coordinate value (Fig.11b).

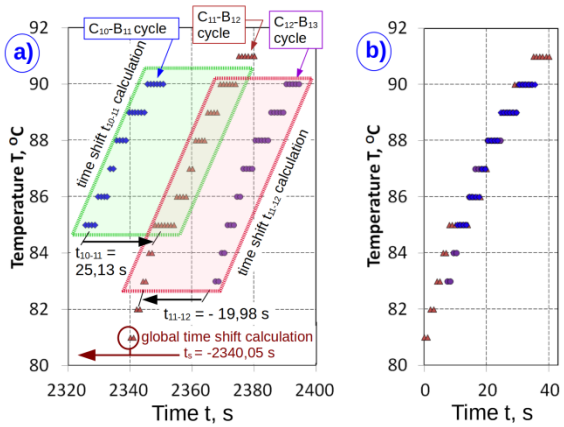

Fig. 11. Scheme for determining time shifts using the example of 3 successive phases of engine temperature increase (CB)

Based on data sets obtained using TimeShift.exe, the different phases of thermostat operation were modelled with continuous functions. To model the engine temperature changes during operation, exponential functions were chosen. The rising temperature curves were described by functions according to equation (5), while the curves with a falling temperature over time were modelled by functions according to equation (6).

$$f_{AB\_i}(t),\ f_{CB\_i}(t) = a_i \cdot \left(1 - e^{-\frac{t+c_i}{b_i}}\right) \tag{5}$$

$$f_{BC\_i}(t) = a_i \cdot e^{-\frac{t+c_i}{b_i}} \tag{6}$$

There are three selectable parameters for these functions. The first two (a_i and b_i) are responsible for the shape of the curve, while the last parameter (c_i) allows the entire curve to be moved along the x-axis of the graph, i.e. the time coordinate t.

The function parameters were calculated using Gnuplot version 5.4.8, since, in addition to the plotting engine, it has an advanced module that allows the declaration of a function and the calculation of its parameters, based on the non-linear Marquardt-Levenberg least squares algorithm. Before calculating the function parameters, it was needed to specify their initial values in advance. The default values for exponential functions in Gnuplot could lead to looping calculations. The calculated parameters (a_i, b_i, c_i) for the nine selected functions, the *RMSE* root mean squared error and the square of the correlation coefficient R^2 of the function with the test data are shown in Table 2.

Looking at Table 2, comparable function parameter values can be observed for the different modelled phases of the engine cooling system between the previously used car $f_{**\_I}(t)$ (shown in blue) and the newer vehicle after repair $f_{**\_III}(t)$ (shown in green). The function parameters for a car with a malfunctioning thermostat f**_II(t), marked in red, are considerably different from those previously mentioned.

Table 2. Function parameters, R^2 and RMSE

	Function	a_i	b_i	c_i	R^2	RMSE
engine warm-up (AB)	$f_{AB\_I}(t)$	158,6	552,3	0,15	0,92	1,37
	$f_{AB\_II}(t)$	171,5	642,9	-0,2	0,94	1,62
	$f_{AB\_III}(t)$	158,7	549,8	0,11	0,94	1,84
cooling phase (BC)	$f_{BC\_I}(t)$	125,3	191,3	5,03	0,74	1,34
	$f_{BC\_II}(t)$	101,4	475,3	5,01	0,80	1,39
	$f_{BC\_III}(t)$	130,7	176,7	5,02	0,71	1,15
warming phase (CB)	$f_{CB\_I}(t)$	100,8	64,1	-3,9	0,81	1,97
	$f_{CB\_II}(t)$	97,0	112,7	99,2	0,86	0,82
	$f_{CB\_III}(t)$	98,3	45,7	2,22	0,80	1,32

In addition, visual representations of the selected functions are shown with the measured data sets. These are shown in Figures 12 and 13. The shades of point colour applied to the visualisations indicate the frequency of occurrence for the data. The darker the colour, the higher the frequency of a data point occurrence. Histograms generated by the Histogram.exe program were used for this purpose. The graphs shown in Figures 12 and 13 were generated using Gnuplot software. Figure 12 displays the selected functions and the corresponding data for the warm-up phase of the cold engine. Similar graphs for the cyclic operation of the thermostat as the engine is warmed up are shown in Figure 13.

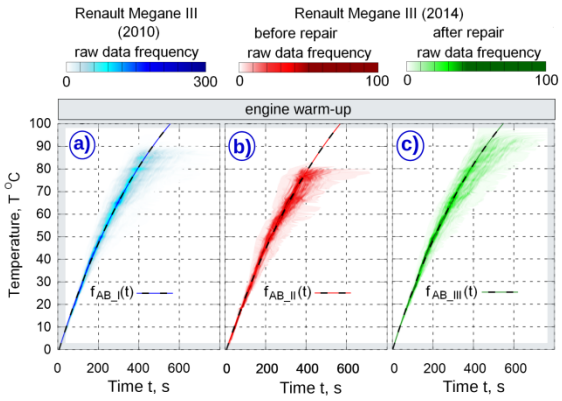

Fig. 12. Functions modelling cold engine warm-up and the frequency of individual data points occurrence

Figures 12 and 13 show that the selected functions adequately represent the characteristics of the measurement data. The functions align with the tops of the histograms, indicating the most common patterns of engine temperature change.

A comparison of the matched functions is shown in Figure 14. Figure 14a displays the comparison for

a cold engine warm-up. Here the AB functions are shown with a range of 0 - 100°C.

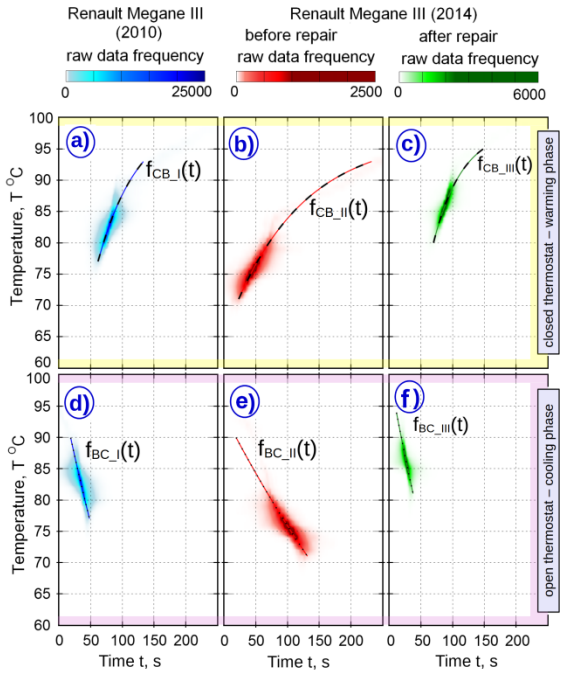

Fig. 13. Functions modelling the cyclic operation of the thermostat and the frequency of individual data points occurrence

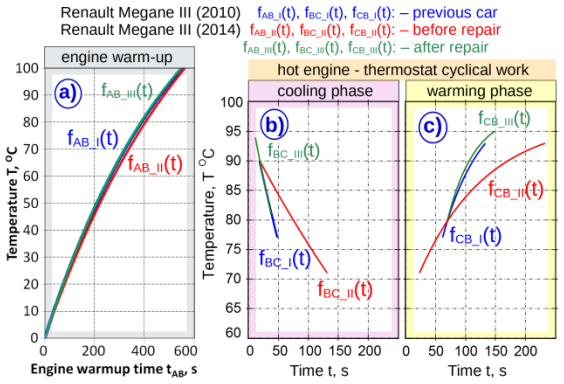

Fig. 14. Comparison of the functions that model changes in the engine temperature over time

From this figure it can be seen that the cold engine warm-up was similar for all the vehicles tested. A closer look reveals that the modelled engine warm-up for the pre-repair vehicle from 0 to 100°C would take approximately 13-16 seconds more than the other cases. This is a difference of less than 3%, which is not considered significant. However, there are significant differences when the engine warms up and the thermostat cycle operation starts. Figures 14b and 14c show this, with the functions plotted over the range of raw data occurrences. It is clear that the cooling phase BC (Fig. 14b) and the warm-up phase CB (Fig. 14c) of the pre-repair car show significant differences (red lines) in comparison with the other two cases. In particular, the pre-repair car has slower heating and cooling processes, as shown by the flatter curves.

The engine heat up and cool down rates were calculated for the pre-selected functions using equation (7).

$$v_i = \frac{dT}{dt} \tag{7}$$

Their minimum $v_{i\ min}$, maximum $v_{i\ max}$ and average $v_{i\ avg}$ were then evaluated (Table 3).

Table 3. Engine warming and cooling rate

	Function	$v_{i\ min}$ [°C/s]	$v_{i\ max}$ [°C/s]	$v_{i\ avg}$ [°C/s]
engine warm-up (AB)	$f_{AB\_I}(t)$	0,100	0,290	0,183
	$f_{AB\_II}(t)$	0,111	0,269	0,179
	$f_{AB\_III}(t)$	0,107	0,289	0,183
cooling phase (BC)	$f_{BC\_I}(t)$	-0,470	-0,403	-0,436
	$f_{BC\_II}(t)$	-0,189	-0,149	-0,169
	$f_{BC\_III}(t)$	-0,532	-0,459	-0,494
warming phase (CB)	$f_{CB\_I}(t)$	0,121	0,370	0,223
	$f_{CB\_II}(t)$	0,036	0,231	0,105
	$f_{CB\_III}(t)$	0,072	0,399	0,191

Table 3 confirms the relationships observed in Figure 14. The average engine warm-up speeds (AB) are similar in the three cases, with differences not exceeding 3%.

An analysis of the cyclical engine cooling and warming rates during thermostat cyclical operation, based on the functions developed, highlights the fundamental difference between cars with a properly functioning thermostat and this with a malfunctioning one. After the replacement of the thermostat in the Renault Megane (2014), the average cyclical engine warm-up (CB) speeds almost doubled and the cyclical cooling speeds almost tripled compared to the state before the replacement.

While compiling the measurement data, information on the time and temperature of all opening (C) and closing (B) points of the thermostat during its cyclic operation was recorded. This was used to calculate the average temperature at which the thermostat opened and closed (Table 4). Typically, the thermostat's first opening temperature T_{B1} is slightly higher than the subsequent cycle opening temperatures T_{Bi}. No similar relationship was found for closing temperatures T_{Ci}. The difference between the thermostat's opening and closing temperatures gives its thermal operating hysteresis, ΔT_{BC}. Their average values are also shown in Table 4.

Based on the average opening and closing temperatures of the thermostat and the functions modelling the different phases of the engine cooling system operation, composite functions have been developed to show the operation of the cooling system in the three cases studied.

Table 4. Values of average temperatures of thermostat cyclical operation closures T_{avgB1}, T_{avgBi}, openings T_{avgCi} and temperature hysteresis ΔT_{BC}

Car	T_{avgB1} [°C]	T_{avgBi} [°C]	T_{avgCi} [°C]	ΔT_{BC} [°C]
Renault Megane III (2010) previous car	88,61	84,83	80,82	4,01
Renault Megane III (2014) before repair	79,72	77,33	74,80	2,53
Renault Megane III (2014) after repair	94,36	88,55	84,07	4,48

By modifying the values of the c_i coefficients in the functions $f_{CB\_*}(t)$ and $f_{BC\_*}(t)$, it is possible to shift them on the time axis. This process results in obtaining composite periodic functions, where temperatures vary within the range of temperatures T_{avgBi} and T_{avgCi}. For the three studied datasets considered, these functions are denoted $f\__I(t)$, $f\__{II}(t)$ and $f\__{III}(t)$. Their plots for a 600 second period after a cold start from 0°C are shown in Figure 15a. Figure 15b shows an enlarged section of the temperature curve of a warmed up engine during the thermostat cyclical operation.

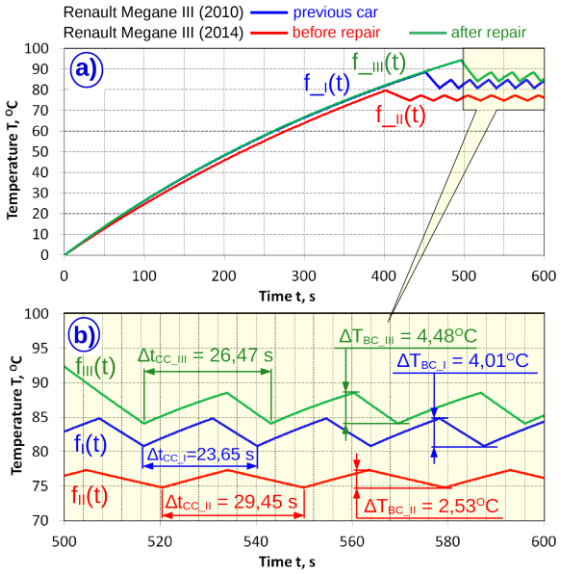

Fig. 15. Comparison of the functions used to model the operation of the cooling system

As shown in Figure 15, the $f\__{II}(t)$ function showing cooling system operation for Renault Megane (2014) before thermostat replacement shows that engine temperature is kept noticeably below 80°C, consistent with observations and measurements. The cooling system maintains a small temperature fluctuations ΔT_{BC_II} estimated at 2.5°C. The temperature fluctuate slowly up and down, producing an average thermostat cycle with a Δt_{CC_II} period of nearly 30 seconds.

The waveform of the $f\__{III}(t)$ function obtained for the post-repair car is very similar to that of the $f\__I(t)$ function for the previously used car. The only noticeable difference is that the engine temperature is slightly higher after the repair. The ranges of the temperature fluctuations are similar, ranging from 4 to 4.5°C, and the thermostat cycle lasts almost 25 seconds in both cases. The data indicate that the failure of the thermostat had the greatest effect on the length of the cooling phase (Δt_{BC}), being about 70% longer than that of the thermostat in a good working order.

Table 5. Time characteristics of models of thermostat cyclic operation

Car	warming phase time Δt_{CB} [s]	cooling phase time Δt_{BC} [s]	thermostat cycle time Δt_{CC} [s]
Renault Megane III (2010) previous car	14,39	9,26	23,65
Renault Megane III (2014) before repair	13,60	15,85	29,45
Renault Megane III (2014) after repair	17,30	9,17	26,47

3.3. Fuel consumption

A symptom of the thermostat malfunction was an increased fuel consumption, particularly noticeable during the winter months when outside temperatures were low. Both the current car and the previous car were filled to full tank throughout their refuellings. This made it possible to calculate the car's fuel consumption each time. Photographs of the vehicle odometer and fuel distributor readings were taken at each refuelling, providing data from which mileage and fuel consumption could be calculated. This analysis was carried out over three different periods of vehicle use. The total distance covered in each period was approximately 7,000 km. Figure 16 displays the mileage and fuel consumption figures.

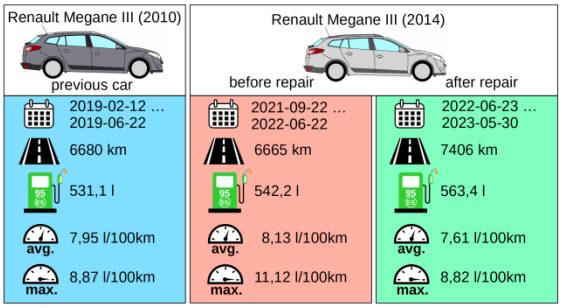

Fig. 16. Basic data on fuel consumption of studied vehicles

Before the repair, the Renault Megane III (2014) in current use had a slightly higher average fuel consumption, which decreased by 6.4% after the repair.

For comparison, the initial period of use of the Renault Megane III (2010) was also taken into account when the engine was fuelled with E95 unleaded gasoline. Later, when the vehicle was fitted with an LPG system, the comparison was made using gasoline only. The average fuel consumption

during this period was 2.2% lower than that of the car with the defective thermostat. Considering the slight variations in mean fuel consumption, it would be uncertain to draw far-reaching conclusions from them. However, significant differences can be observed when analysing the calculated average fuel consumption between refuellings, as shown in Figure 17.

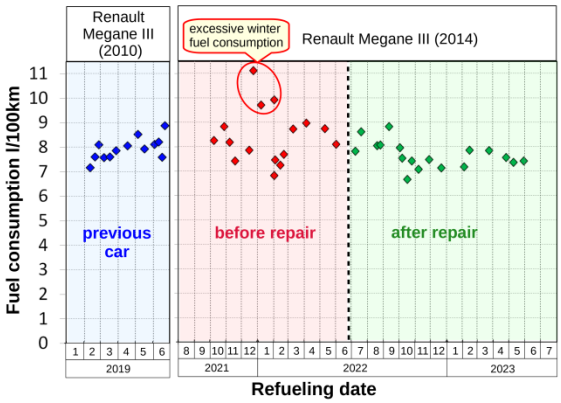

Fig. 17. Fuel consumption between refuellings

The vehicle with a defective thermostat consumed 10 - 11 l/100km in low outside temperature conditions, while the usual fuel consumption for similar driving was between 7 and 9 l/100km. This means that the difference in the maximum fuel consumption values recorded was more than 25 %. It should be noted that significantly lower fuel consumption was also recorded in January/February 2022. However, the recorded driving logs show that several hundred kilometres of motorway and expressway were driven during this period. These journeys took place in atmospheric conditions that required speed maintained within a range of approximately 80-90 km/h, resulting in a low fuel consumption rate.

After replacing the thermostat with a new one, fuel consumption never exceeded 8.82 l/100 km, regardless of the season or outside temperature. The sharp rise in fuel prices also led to changes in driving behaviour, such as increased use of cruise control and modified driving style. This trend can be seen since October 2022 in Figure 17, where the average fuel consumption between refuellings does not exceed 8 l/100 km.

4. CONCLUSIONS

The proper functioning of the cooling system in an internal combustion engine is crucial for removing excess heat energy and maintaining its temperature for optimal lubrication. Therefore, it is rather surprising to see the limited capabilities of the automatic diagnostics built into the ECUs of the cars tested. By using an OBD-II interface and commonly available technical components, these capabilities can be significantly enhanced. It is often possible to diagnose problems more accurately and detect faults that the ECU hasn't reported as faults by continuously analysing the data downloaded from the ECU. To identify a fault in the cooling system, continuous monitoring of the engine temperature histogram and its changes may be sufficient. The median of the engine temperature is an effective parameter for diagnosis. This parameter is less affected by the warming up of a cold engine than the average value. The algorithms used to calculate the median and the engine temperature histogram require minimal memory and computing power, and should be easy for car manufacturers to incorporate into their ECU control programs.

The thermostat malfunction in the 2014 Renault Megane III was verified by basic statistical analysis of the collected engine temperature measurements and the repair was confirmed to be correct.

The replacement of the defective thermostat led to an increase of the coolant temperature during engine operation of approximately 10°C, which was confirmed by the basic data statistics and thermostat cycle analysis (Refer to Table 4). In addition, during its cyclic operation, the defective thermostat caused the signifficant decrease of thermal hysteresis of the cooling system ΔT_{BC}.

By modelling the operation of the cooling system using mathematical functions, it was possible to carry out a more detailed analysis of the thermostat malfunction. By comparing the obtained functions, it was possible to identify a significant symptom of thermostat malfunction, which was a reduction in the cooling and heating rate of the engine. This problem occurred after the cold engine had warmed up, when the thermostat started cycling to stabilise the temperature. The most noticeable difference is in the rate of temperature drop during the cooling phase BC of the engine, which is almost three times smaller than with a properly functioning thermostat. During the warming phase CB of the engine, the thermostat in good working order enabled about twice the heating up speed. Indicators of a malfunctioning thermostat suggest that it partially opens at lower than optimum temperatures and remains open at varying degrees during cycling. This explains the low engine temperatures, their small range and how slow they tend to change.

An increase in the car's fuel consumption may indicate the need for a car diagnosis. However, it must be remembered that several operational factors influence this. After replacing the thermostat, the abnormally high fuel consumption did not occur again, confirming the diagnostic process carried out and the accuracy of the repair.

Author contributions: *research concept and design, K.W., M.W.; Collection and/or assembly of data, (K.W.; Data analysis and interpretation, K.W., M.W.; Writing the article, K.W., M.W.; Critical revision of the article, K.W., M.W.; Final approval of the article, K.W., M.W.*

Declaration of competing interest: *The authors declare that they have no known competing financial interests or personal relationships that could have appeared to influence the work reported in this paper.*

REFERENCES

1. Agarwal N., Chiara F., Canova M. Control-Oriented Modeling of an Automotive Thermal Management System. 2012 Workshop on Engine and Powertrain Control, Simulation and Modeling. The International Federation of Automatic Control Rueil-Malmaison, France, October 23-25, 2012: 392-399. https://doi.org/10.3182/20121023-3-FR-4025.00051.
2. Aliramezani M., Koch Ch. R., Patrick R. Phenomenological model of a solid electrolyte NO_x and O_2 sensor using temperature perturbation for on-board diagnostics. Solid State Ionics 2018; 321: 62-68. https://doi.org/10.1016/j.ssi.2018.04.004.
3. Basir H., Hosseini S.A., Nasrollahnezhad S., Jahangiri A., Rosen M.A. Investigation of engine's thermal management based on the characteristics of a map-controlled thermostat. International Communications in Heat and Mass Transfer 2022; 135: 106156. https://doi.org/10.1016/j.icheatmasstransfer.2022.106156.
4. Becker M., Czech P., Gustof P., Turoń K., Jędrusik D., Urbańczyk R. Operation of the car in winter conditions. Autobusy 2017; 12: 701-708. Polish. https://doi.org/10.24136/atest.2017.658.
5. Caban J., Droździel P., Ignaciuk P., Kordos P. The impact of changing the fuel dose on chosen parameters of the diesel engine start-up process. Transport Problems 2019; 14 (4): 51- 62. https://doi.org/10.20858/tp.2019.14.4.5.
6. Cardenas Contreras E.M., Bandarra Filho E.P. Heat transfer performance of an automotive radiator with MWCNT nanofluid cooling in a high operating temperature range. Applied Thermal Engineering 2022; 207: 118149. https://doi.org/10.1016/j.applthermaleng.2022.118149.
7. Cardenas Contreras E.M., Oliveira G.A., Bandarra Filho E.P. Experimental analysis of the thermohydraulic performance of graphene and silver nanofluids in automotive cooling systems. International Journal of Heat and Mass Transfer 2019;132:375–387. https://doi.org/10.1016/j.ijheatmasstransfer.2018.12.014.
8. Chaurasiya R., Krishnasamy A. A single fuel port and direct injected low temperature combustion strategy to reduce regulated pollutants from a light-duty diesel engine. Fuel 2023; 335: 127114. https://doi.org/10.1016/j.fuel.2022.127114.
9. Chipman J.C., Houtz W., Shillor M. Simulations of a Thermostat Model I: Approach to Steady States. Mathematical and Computer Modelling 2000; 32: 765-790. https://doi.org/10.1016/S0895-7177(00)00170-9.
10. Costin M.H. On-Board Diagnostics of Vehicle Emission System Components: Review of Upcoming Government Regulation. IFAC Proceedings Volumes 1991;24 (6):497-501. https://doi.org/10.1016/S1474-6670(17)51190-8.
11. Gorzelanczyk P., Jurkovic M., Kalina T., Sosedova J., Luptak V. Influence of motorization development on civilization diseases. Transport Problems 2020; 15 (3): 53-66. https://doi.org/10.21307/tp-2020-033.
12. He X., Zhou Y., Liu Z., Yang Q., Sjöberg M., Vuilleumier D., Ding C.P., Liu F. Impact of coolant temperature on the combustion characteristics and emissions of a stratified-charge direct-injection spark-ignition engine fueled with E30. Fuel 2022; 309: 121913. https://doi.org/10.1016/j.fuel.2021.121913.
13. Kubica G. An influence of load on temperature of combustion chamber walls in SI engine. Scientific Journal of Silesian University of Technology. Series Transport 2010; 66: 57-64. https://doi.org/10.20858/sjsutst.2010.66.6.
14. Leong K.Y., Saidur R., Kazi S.N., Mamun A.H. Performance investigation of an automotive car radiator operated with nanofluid-based coolants (nanofluid as a coolant in a radiator). Applied Thermal Engineering 2010; 30: 2685-2692. https://doi.org/10.1016/j.applthermaleng.2010.07.019.
15. Ma Q., Zhang Q., Chen Z., Liang J. The energy analysis and performance of heavy-duty diesel engine with n-butanol addition and different coolant temperature. Fuel 2022; 316: 123323. https://doi.org/10.1016/j.fuel.2022.123323.
16. Mohamed E.S. Development and analysis of a variable position thermostat for smart cooling system of a light duty diesel vehicles and engine emissions assessment during NEDC. Applied Thermal Engineering 2016; 99: 358–372. https://doi.org/10.1016/j.applthermaleng.2015.12.099.
17. Puškár, M., Lavčák, M., Šoltésová, M., Kopas, M. Analysis of advanced technology for combustion of homogeneous fuel mixture. Scientific Journal of Silesian University of Technology. Series Transport. 2022; 117: 211-220. https://doi.org/10.20858/sjsutst.2022.117.14.
18. Ramírez J.D., Romero C.A., Mejía J.C., Quintero H.F. A methodology for non-invasive diagnosis of diesel engines through characteristics of starter system performance. Diagnostyka 2022; 23(2): 2022202. https://doi.org/10.29354/diag/147789.
19. Ryniewicz A.M., Bojko Ł., Madej T. The estimation of lubricity and viscosity of engine oils. Diagnostyka 2014; 15(1): 61-66.
20. Sakno, O., Medvediev, I., Kolesnikova, T. Study on the relationship between vehicle maintenance and fuel consumption. Scientific Journal of Silesian University of Technology. Series Transport. 2021; 113:163-172. https://doi.org/10.20858/sjsutst.2021.113.13.
21. Salah M.H., Frick P.M., Wagner J.R., Dawson D.M. Hydraulic actuated automotive cooling systems—Nonlinear control and test. Control Engineering Practice 2009; 17: 609–621. https://doi.org/10.1016/j.conengprac.2008.10.016.
22. Singh V., Rijpkema J.J., Munch K., Andersson S.B., Verhelst S. On the effects of increased coolant temperatures of light duty engines on waste heat recovery. Applied Thermal Engineering 2020; 172: 115157. https://doi.org/10.1016/j.applthermaleng.2020.115157.
23. Walentynowicz J., Krakowski R. Modeling of the higher pressure cooling system for transport vehicles engines. Transport Problems 2010; 5(4): 39-47. https://doi.org/10.20858/tp.2010.5.4.5.
24. Wang T., Wagner J. Advanced automotive thermal management – Nonlinear radiator fan matrix control.

Control Engineering Practice 2015; 41: 113–123. https://doi.org/10.1016/j.conengprac.2015.04.004.
25. Yang L., Zhang S., Wu Y., Chen Q., Niu T., Huang X., Zhang S., Zhang L., Zhou Y., Hao J. Evaluating real-world CO_2 and NO_X emissions for public transit buses using a remote wireless on-board diagnostic (OBD) approach. Environmental Pollution 2016; 218: 453-462. https://doi.org/10.1016/j.envpol.2016.07.025.
26. Zarda F, Hussein AM, Danook AH, Mohamad B. Enhancement of thermal efficiency of nanofluid flows in a flat solar collector using CFD. Diagnostyka 2022; 23(4): 2022411. https://doi.org/10.29354/diag/156384.

Kazimierz WITASZEK received M.Sc. and PhD degrees in transport, from the Silesian University of Technology (SUT). He works on the Faculty of Transport and Aviation Engineering. His research is focused on measurement, data processing, artificial neural networks in automotive sector.

Mirosław WITASZEK obtained his Ph.D. degree at the Transport Department of the Silesian University of Technology in Katowice in the field of Machine Construction and Operation. His field of research – tribology, life and reliability of the elements of vehicles.